A multiscale model for glioma spread including cell-tissue interactions and proliferation

Christian Engwer, Markus Knappitsch, Christina Surulescu

April 7, 2014

Abstract

Glioma is a broad class of brain and spinal cord tumors arising from glia cells, which are the main brain cells that can develop into neoplasms. Since they are highly invasive they are hard to remove by surgery, as the tumor margin it most often not precisely enough identifiable. The understanding of glioma spread patterns is hence essential for both radiological therapy as well as surgical treatment. In this paper we propose a multiscale model for glioma growth including interactions of the cells with the underlying tissue network, along with proliferative effects. As in [12], we assume that cancer cells use neuronal fibre tracts as invasive pathways. Hence, the individual structure of brain tissue seems to be decisive for the tumor spread. Diffusion tensor imaging (DTI) is able to provide such information, thus opening the way for patient specific modelling of glioma invasion. Starting from a multiscale model involving subcellular (microscopic) and individual (mesoscale) cell dynamics, we do a parabolic scaling to obtain an approximating reaction-diffusion-transport equation on the macroscale of the tumor cell population and perform numerical simulations based on DTI data in order to assess the performance of our modeling approach.

1 Introduction

Gliomas are malignant primary tumors in the human brain with a poor prognosis [37]. The common treatment approach involves surgical resection, usually followed by radiotherapy. Thereby, the assessment of the tumor margin is, however, a challenging issue, due to the high invasiveness of gliomas and their finger-like, often disconnected patterns. Mathematical models aim at providing enhanced information about position, shape, and extent of the tumor by relying on medical imaging techniques. In particular, diffusion tensor imaging (DTI) is one of the most common radiological methods in the detection of brain tumors [32]. On T1- and T2-weighted images neoplastic and healthy tissue differ in intensity, thus making the core part of the tumor visible.

DTI techniques are non-invasive and they permit to assess the specific brain architecture. Modern imaging methods rely on evaluating the diffusion behaviour of water molecules within structured tissue. This reveals the orientation and anisotropy (meaning the extent to which fibers align together) of neuronal fibers making up white matter tracts. This information is particularly interesting for surgical and radiation therapy.

Several key features have been identified to be crucial for tumor progression, see e.g., [17]. In this work we focus on the interaction of tumor cells with the underlying tissue and on proliferative effects. The model we propose here has a multiscale character, with the purpose of connecting the various levels on which the relevant biochemical processes triggering glioma spread take place. For modeling tumor growth we rely on the *go-or-grow* hypothesis, which states that cancer cells can either move or proliferate [15, 21]. We assume that cancer cells use neuronal fibre tracts as invasive pathways, which makes the individual brain structure interesting for patient specific modelling of glioma. Diffusion tensor imaging data are able to provide this information [34, 35].
Starting in Section 2 with a kinetic model on the mesoscale and an ODE on the subcellular level, a parabolic scaling yields an approximating reaction-diffusion-transport equation on the macroscale. Thereby, the precise form of the coefficients is determined by using DTI data. Section 3 is concerned with the numerical simulation of the macroscopic equation. Eventually, in Section 4 we comment on the performance of this modeling approach.

1.1 Multiscale modelling of glioma growth

The invasion of tumor cells is a highly complex process involving a plethora of phenomena on different spatial and temporal scales [17]. Multiscale models can help to map this high degree of complexity into mathematical structures. Such mathematical settings involve two or several scales and accordingly more or less details of the processes they describe. Micro-macro models for tumor cell migration have been proposed and analysed e.g., in [28], which accounts for the effect of heat shock proteins (microlevel) on cancer invasion (on the macrolevel) and extends the model in [33], or more recently for the migration of cancer cells performing haptotaxis and chemotaxis (macroscale) under the influence of integrin binding to soluble and unsoluble ligands (microscale) [27, 30] or for the acid-mediated tumor invasion with pH taxis [31]. Different, but related approaches are hybrids between discrete and continuous modeling. These use cellular Potts or (lattice gas) cellular automata to provide lattice based simulations of individual cells involving more or less details on the subcellular level, from which information about the behavior on the population level can be extracted, see e.g., [8, 18] and the references therein. More complex continuum models also involving mesoscale dynamics (individual cell-tissue and/or cell-cell interactions) were considered by Bellomo et al. [4, 5, 6] or -fitting in the same framework- in e.g., [12, 22, 23, 26].
In our model for glioma growth and spread we distinguish between three different scales. The *microscale* refers to processes happening on the subcellular level. In our setting these reduce to the binding of cell surface receptors to unsoluble ligands (proteins on the myelinated axon fibers) and employs an ordinary differential equation for the corresponding mass action kinetics. The *mesoscale* accounts for the behavior of individual cells and their interactions with their surroundings, in this case the (anisotropic) tissue network. The dynamics are characterized with the aid of kinetic transport equations for the densities of moving and resting cells (see Section 2.3). At this point, we rely on the above mentioned *go or grow* hypothesis. Finally, the *macroscale* refers to the population level on which the tumor as a whole can be observed. Unlike the previous two scales, it is not contained in the original model, but deduced from it. More precisely, it is our goal in this paper do derive an equation for the macroscopic density $N(t, \mathbf{x})$ of tumor cells at time t at position $\mathbf{x}$, which also contains the information of the descriptions of the micro- and mesoscales.

1.2 Diffusion tensor imaging

At present, medical imaging methods like *computed tomography* (CT) along with magnetic resonance imaging based methods like *diffusion tensor imaging* (DTI) play a central role in the diagnosis of brain tumors in general. Cancerous tissue and healthy tissue differ in intensity in the representation, and hence malignant tissue alterations can be observed. One significant shortcoming is that not the whole tumor is visible, but only its core part. The actual tumor margin cannot be assessed. This is a large drawback, since after resection of the malignant region visible on DTI or CT scans the tumor can start growing again due to the incomplete removal.
However, in particular the diffusion tensor imaging (DTI) method is of high value for glioma prognosis as it provides information about the local tissue strcuture within the brain [35]. DTI relies on the measurement of the diffusion behaviour of water molecules within structured tissue, relating it to the anisotopy of neural fibre tracts [9, 34]. The water molecules are assumed to diffuse faster along fibre structures than orthogonally to them, which allows to capture the mentioned anisotropy. Technically, DTI measures the aparrent diffusivity of water molecules per volume element (voxel). This can be characterized with a symmetric tensor, the *water diffusion tensor*

$$\mathbb{D}_W(\mathbf{x}) = \begin{pmatrix} d_{xx}(\mathbf{x}) & d_{xy}(\mathbf{x}) & d_{xz}(\mathbf{x}) \\ d_{yx}(\mathbf{x}) & d_{yy}(\mathbf{x}) & d_{yz}(\mathbf{x}) \\ d_{zx}(\mathbf{x}) & d_{zy}(\mathbf{x}) & d_{zz}(\mathbf{x}) \end{pmatrix}. \tag{1}$$

Thereby, the diffusion tensor can be visualized e.g., with the aid of the *fractional anisotropy index* [7] or with *tensor glyphs*. While the former is a scalar value between zero and one, computed by using the eigenvalues of the apparent diffusion tensor[1], the latter convey tensor variables by mapping the tensor eigenvectors and eigenvalues to the orientation and shape of e.g., a cuboid or an ellipsoid. Glyphs commonly used in this context are *ellipsoids* and *peanuts*. For more details on this topic we refer to [12] and the references therein.
Tractography aims to reconstruct the local tissue orientation out of DTI data [10, 11]. This is a quite

[1] A value close to one means high anisotropy, i.e., a strong preference for a specific direction, whereas a very small value corresponds to the nearly isotropic case.

complex process and still part of ongoing research. As we are primarily interested in one main direction of tissue fibres per voxel, we will use a simple mathematical expression to connect the water diffusion tensor and the local fibre distribution in Section 2.4.

2 A multiscale model including proliferation

2.1 Transport equations with resting phases

We aim at providing a multiscale model for glioma spread wich includes proliferation and interactions of the cells with the extracellular matrix. It has been proposed that the go-or-grow hypothesis is a good starting point in modeling proliferative effects on the cell scale [8, 18]. Here we start from the approach in [19] and propose a setting which is expanded by a model for the cell receptor dynamics on the microscale as in [12] and which also accounts for the interaction between tumor cells and tissue fibres.
We aim at observing the density functions $p(t, \mathbf{x}, \mathbf{v}, \mathbf{y})$ of moving cells at time t, position $\mathbf{x} \in \mathbb{R}^n$, velocity $\mathbf{v} \in V \subset \mathbb{R}^n$, and internal state $\mathbf{y} \in Y \subset \mathbb{R}^d$ and of resting (and hence proliferating) cells $r(t, \mathbf{x}, \mathbf{y})$. This leads to a system of equations of the form

$$\partial_t p + \nabla_{\mathbf{x}} \cdot (\mathbf{v}p) + \nabla_{\mathbf{y}} \cdot (\mathbf{G}(\mathbf{y})p) = \mathcal{L}[\lambda]p - \alpha(\mathbf{x})p + \frac{\beta q}{\omega} r - l(N)p, \tag{2}$$

$$\partial_t r = \alpha(\mathbf{x}) \int_V p d\mathbf{v} - \beta r + g(N)r - l(N)r. \tag{3}$$

Here $\mathcal{L}[\lambda]p := -\lambda(\mathbf{y})p + \lambda(\mathbf{y}) \int_V K(\mathbf{x}, \mathbf{v})p(\mathbf{v}')d\mathbf{v}'$ is the *turning operator* modeling the cell velocity innovations due to contact guidance, environmental cues etc. These influences are contained in the turning kernel K. As in [12], we choose $K(\mathbf{x}, \mathbf{v}) = \frac{q(\mathbf{x}, \hat{\mathbf{v}})}{\omega}$, where $\hat{\mathbf{v}}$ is the normalized velocity, $q(\mathbf{x}, \hat{\mathbf{v}})$ is the directional distribution of tissue fibers, and $\omega = \int_V q(\hat{\mathbf{v}})d\mathbf{v} = s^{n-1}$ is a scaling constant. The function $\lambda(\mathbf{y})$ denotes the *turning rate* of cells. The vector $\mathbf{y}$ stands for the internal state of a cell: its components can be, for instance, concentrations of proteins involved in some intracellular signaling network or -as will be the case throughout this work- the concentration of integrins bound to tissue fibres in the cell environment. Its dynamics is characterized by a system of ordinary differential equations

$$\frac{d}{dt}\mathbf{y}(t) = \mathbf{G}(\mathbf{y}(t), A), \tag{4}$$

where the right hand side is involving the volume fraction of tissue $A(t, \mathbf{x})$ (including ECM and brain fibers) as input, see [12]. For simplicity we account in this work only for binding of cell surface receptors to unsoluble components on the tissue, modeled by A. This assumption reduces the above ODE system to just one equation for the receptor binding dynamics, see (6) below.
The function N in equations (2) and (3) denotes the total cell density and is given by

$$N(t, \mathbf{x}) = \int_V \int_Y p(t, \mathbf{x}, \mathbf{v}, y)dy \; d\mathbf{v} + \int_Y r(t, \mathbf{x}, y)dy, \tag{5}$$

and $g(N)$ and $l(N)$ are functions representing *gain* and *loss* due to cell death and proliferation. α and β are the rates with which cells stop and proliferate, respectively start moving after a resting (proliferating) phase. Thereby, the cells which exit the proliferative phase and start to move are doing this by interacting with the tissue. [2] Both α and β depend on the position $\mathbf{x}$.

2.2 Cell surface receptor dynamics

As in [12], we focus on the cell surface receptor dynamics of the cells. Transmembrane adhesion proteins bind to unsoluble proteins in the brain tissue. In this work we want to study the impact of this microscopic process on the macroscopic movement behaviour on the tissue scale. Starting from simple mass action kinetics, the receptor binding dynamics on the cell surface is described by the following ordinary differential equation:

$$\dot{y} = k^+(R_0 - y)A - k^- y, \tag{6}$$

where R_0 denotes the total number of receptors on the cell (we assume it is conserved), whereas $y(t)$ gives the density of integrins bound to ECM fibres. The constants k^+ and k^- denote the reaction rates

[2] The importance of cell-tissue interactions (via receptor bindings to the nonsoluble ligands on the tissue fibers) for cell division has been experimentally put in evidence, see e.g., [25].

for the reversible binding of integrins to the tissue fibres. The steady state of equation (6) is given by $y^* = \frac{k^+ A R_0}{k^+ A + k^-}$. Following[12] we introduce a new internal variable $z := y^* - y$ measuring deviations from the steady state. Next consider the path of a single cell starting in $\mathbf{x}_0$ and moving with velocity $\mathbf{v}$ through a time-invariant density field $A(\mathbf{x})$. Then with the notations $\mathbf{x} = \mathbf{x}_0 + \mathbf{v}t$ and

$$f(A(\mathbf{x})) = \frac{k^+ A(\mathbf{x}) R_0}{k^+ A(\mathbf{x}) + k^-} \tag{7}$$

it follows that for any t

$$\frac{d}{dt} f\big(A(\mathbf{x}_0 + \mathbf{v}t)\big) = f'(A(\mathbf{x}_0 + \mathbf{v}t))\ \mathbf{v} \cdot \nabla A(\mathbf{x}_0 + \mathbf{v}t)$$

and hence z satisfies the equation

$$\begin{aligned} \dot{z} &= -(k^+ A(\mathbf{x}) + k^-) z + f'(A(\mathbf{x})) \mathbf{v} \cdot \nabla A(\mathbf{x}) \\ &= -(k^+ A(\mathbf{x}) + k^-) z + \frac{k^+ k^- R_0}{(k^+ A(\mathbf{x}) + k^-)^2}\ \mathbf{v} \cdot \nabla A(\mathbf{x}). \end{aligned} \tag{8}$$

This equation can be solved explicitly for z to yield

$$z(t) = (y^* - y_0) e^{-(k^+ A + k^-)t} + (1 - e^{-(k^+ A + k^-)t}) \frac{k^+ k^- R_0}{(k^+ A + k^-)^3}\ \mathbf{v} \cdot \nabla A,$$

where $y_0 = y(0)$. Hence, z is bounded as long as ∇A it is and its sign depends on the current orientation of the cell w.r.t. the gradient of the fibre volume fraction.

We choose the turning rate to be of the form $\lambda(z) = \lambda_0 - \lambda_1 z \geq 0$, where λ_0 and λ_1 are some positive constants with $\lambda_0 \geq \lambda_1 R_0 (1 - \frac{1}{K_r A(\mathbf{x}) + 1})$ and $K_r := k^+ / k^-$. Note that this is equivalent to considering $\lambda(y) = \lambda_0 - \lambda_1 y^* + \lambda_1 y$, which becomes indeed larger when many receptors are bound to fibres. This choice corresponds to the one proposed in [13] for the turning rate of bacteria and -after a linearization- also to that chosen in [16]. Further, observe that z involves the spatial position $\mathbf{x}$ of the cell as a parameter and there exists $z_{\max} = \max_{\mathbf{x} \in \mathbb{R}^n} z > 0$. Choosing $\lambda_1 \leq \min \left\{ \frac{\lambda_0}{z_{\max}}, \sup_{\mathbf{x}} \frac{K_r A + 1}{R_0 K_r A} \right\}$ ensures that $\lambda(z) \geq 0$.

2.3 The mesoscopic transport equation and its scaling

With the above analysis for the dynamics on the microscale, we obtain now a system of evolution equations for the density $p(t, \mathbf{x}, \mathbf{v}, z)$ of moving cells and the density $r(t, \mathbf{x}, z)$ of resting cells. The system reads

$$\partial_t p + \mathbf{v} \cdot \nabla p + \partial_z \left(\left(-(k^+ A + k^-) z + f'(A) \mathbf{v} \cdot \nabla A \right) p \right) = \mathcal{L}[\lambda_0] p + \mathcal{L}[\lambda_1] z p - \alpha(\mathbf{x}) p + \frac{q\beta}{\omega} r - l(N) p \tag{9}$$

$$\partial_t r = \alpha(\mathbf{x}) \int_V p d\mathbf{v} - \beta r + (g(N) - l(N))\, r. \tag{10}$$

Introduce the notations

$$m = \int_Z p dz, \quad w = \int_Z r dz \tag{11}$$

$$m^z = \int_Z z p dz, \quad w^z = \int_Z z r dz \tag{12}$$

$$M = \int_V m d\mathbf{v}, \quad M^z = \int_V m^z d\mathbf{v}, \tag{13}$$

where $Z \subseteq [y^* - R_0, y^*]$ is our new domain for the internal dynamics. In the following we assume the data to be compactly supported in the $(\mathbf{x}, \mathbf{v}, z)$-space, which allows to perform the subsequent calculations. Integration of the equations (9) and (10) with respect to z gives

$$\partial_t m + \mathbf{v} \cdot \nabla m = \mathcal{L}[\lambda_0] m + \mathcal{L}[\lambda_1] m^z - \alpha m + \frac{\beta q}{\omega} w - l(N) m, \tag{14}$$

$$\partial_t w = \alpha(\mathbf{x}) M - \beta w + (g(N) - l(N))\, w. \tag{15}$$

Multiply equations (9) and (10) by z and integrate again with resp. to z. As in [12] we neglect moments of higher order in z and obtain

$$\partial_t m^z + \mathbf{v}\cdot\nabla m^z = -(k^+A + k^-)m^z + f'(A)\mathbf{v}\cdot\nabla A\; m + \mathcal{L}[\lambda_0]m^z - \alpha m^z + \frac{\beta q}{\omega}w^z - l(N)m^z, \tag{16}$$

$$\partial_t w^z = \alpha\int M^z - \beta w^z + g(N)w^z - l(N)w^z. \tag{17}$$

Now, we use a parabolic scaling $\hat{t}\to\varepsilon^2 t$, $\hat{\mathbf{x}}\to\varepsilon\mathbf{x}$, then drop the hats for notational simplification. In addition, we scale the birth-death dynamics as in [19] by

$$g(N)\to\varepsilon^2\hat{g}(\hat{N}) \tag{18}$$

$$l(N)\to\varepsilon^2\hat{l}(\hat{N}). \tag{19}$$

This scaling relies on the assumption that the time scale on which birth and death events occur is much slower than the random walk process. From equations (14), (15), (16) and (17) we obtain

$$\varepsilon^2\partial_t m + \varepsilon\mathbf{v}\cdot\nabla m = \mathcal{L}[\lambda_0]m + \mathcal{L}[\lambda_1]m^z - \alpha m + \frac{\beta q}{\omega}w - \varepsilon^2 l(N)m, \tag{20}$$

$$\varepsilon^2\partial_t w = \alpha(\mathbf{x})M - \beta w + \varepsilon^2\left(g(N) - l(N)\right)w, \tag{21}$$

$$\varepsilon^2\partial_t m^z + \varepsilon\mathbf{v}\cdot\nabla m^z = -(k^+A + k^-)m^z + \varepsilon f'(A)\mathbf{v}\cdot\nabla A\; m + \mathcal{L}[\lambda_0]m^z - \alpha m^z + \frac{\beta q}{\omega}w^z - \varepsilon^2 l(N)m^z, \tag{22}$$

$$\varepsilon^2\partial_t w^z = \alpha M^z - \beta w^z + \varepsilon^2\left(g(N) - l(N)\right)w^z. \tag{23}$$

Now, we use Hilbert expansions for m, m^z, w, w^z, M, M^z of the form

$$\begin{aligned} m &= m_0 + \varepsilon m_1 + \varepsilon^2 m_2 + \dots, \quad & M &= M_0 + \varepsilon M_1 + \varepsilon^2 M_2 + \dots \\ m^z &= m_0^z + \varepsilon m_1^z + \varepsilon^2 m_2^z + \dots, \quad & M^z &= M_0^z + \varepsilon M_1^z + \varepsilon^2 M_2^z + \dots \\ w &= w_0 + \varepsilon w_1 + \varepsilon^2 w_2 + \dots, \quad & w^z &= w_0^z + \varepsilon w_1^z + \varepsilon^2 w_2^z + \dots \end{aligned}$$

and compare terms of equal order in ε.

ε^0:

$$0 = \mathcal{L}[\lambda_0]m_0 + \mathcal{L}[\lambda_1]m_0^z - \alpha m_0 + \frac{\beta q}{\omega}w_0, \tag{24}$$

$$0 = \alpha M_0 - \beta w_0, \tag{25}$$

$$0 = -(k^+A + k^-)m_0^z - \alpha m_0^z + \frac{\beta q}{\omega}w_0^z + \mathcal{L}[\lambda_0]m_0^z, \tag{26}$$

$$0 = \alpha M_0^z - \beta w_0^z. \tag{27}$$

ε^1 :

$$\mathbf{v}\cdot\nabla m_0 = \mathcal{L}[\lambda_0]m_1 + \mathcal{L}[\lambda_1]m_1^z - \alpha m_1 + \frac{\beta q}{\omega}w_1, \tag{28}$$

$$0 = \alpha M_1 - \beta w_1, \tag{29}$$

$$\mathbf{v}\cdot\nabla m_0^z = -(k^+A + k^-)m_1^z + f'(A)\mathbf{v}\cdot\nabla A\; m_0 + \mathcal{L}[\lambda_0]m_1^z - \alpha m_1^z + \frac{\beta q}{\omega}w_1^z, \tag{30}$$

$$0 = \alpha M_1^z - \beta w_1^z. \tag{31}$$

ε^2 :

$$\partial_t m_0 + \mathbf{v}\cdot\nabla m_1 = \mathcal{L}[\lambda_0]m_2 + \mathcal{L}[\lambda_1]m_2^z - \alpha m_2 + \frac{\beta q}{\omega}w_2 - l(N_0)m_0, \tag{32}$$

$$\partial_t w_0 = \alpha M_2 - \beta w_2 + \left(g(N_0) - l(N_0)\right)w_0. \tag{33}$$

It is our goal now to derive an evolution equation for the macroscopic cell density

$$N_0(t,\mathbf{x}) = w_0 + M_0 = \left(1 + \frac{\alpha}{\beta}\right)M_0. \tag{34}$$

We start with the equations for the coefficients of ε^0. First of all, we obtain from (27) that $w_0^z = \frac{\alpha}{\beta} M_0^z$. Integration of (26) with respect to $\mathbf{v}$ yields

$$0 = -(k^+ A + k^-) M_0^z - \alpha M_0^z + \beta w_0^z, \tag{35}$$

which implies $M_0^z = 0$, $m_0^z = 0$ and $w_0^z = 0$. Equation (25) gives

$$w_0 = \frac{\alpha}{\beta} M_0. \tag{36}$$

Finally, we obtain from (24)

$$0 = \mathcal{L}[\lambda_0] m_0 - \alpha m_0 + \frac{q\alpha}{\omega} M_0, \text{ from which } m_0 = \frac{q}{\omega} M_0. \tag{37}$$

Now let us analyze the equations for the coefficients of ε^1. Starting with eq. (31) we obtain

$$w_1^z = \frac{\alpha}{\beta} M_1^z. \tag{38}$$

From equation (30) we obtain after integration with respect to $\mathbf{v}$ that $M_1^z = 0$ and hence also $w_1^z = 0$. Here, we used the assumption $\int \mathbf{v} q \; d\mathbf{v} = 0$ for undirected tissue. Then, again from (30) we obtain the following expression for m_1^z:

$$m_1^z = \frac{1}{k^+ A + k^- + \lambda_0 + \alpha} f'(A) \mathbf{v} \cdot \nabla A \; m_0. \tag{39}$$

Equation (28) leads to the expression

$$\mathbf{v} \cdot \nabla m_0 = \mathcal{L}[\lambda_0 + \alpha] m_1 - \lambda_1 m_1^z.$$

Now use the properties of the operator $\mathcal{L}[\lambda_0 + \alpha]$ defined on the weighted L^2-space $L_q^2(V)$. Thereby, the weight function is $q^{-1}(\hat{\mathbf{v}})$ and $\mathcal{L}[\lambda_0 + \alpha]$ is a compact Hilbert-Schmidt operator (see [20]) whose kernel is given by the linear space $\langle q \rangle$, denoting the subspace of $L_q^2(V)$ spanned by q. The pseudoinverse $\mathcal{L}[\lambda_0 + \alpha]^{-1}_{|<q>^\perp}$ of this operator is (see again [20] or [12]) is just the multiplication by the factor $-\frac{1}{\lambda_0 + \alpha}$. This leads to

$$m_1 = -\frac{1}{\lambda_0 + \alpha} \left(\mathbf{v} \cdot \nabla m_0 + \lambda_1 m_1^z \right). \tag{40}$$

Using equations (32) and (33) we can derive an evolution equation for the macroscopic cell density (34). From (33) we have

$$\frac{\beta}{\omega} w^z = \frac{1}{\omega} \left(\alpha M_2 + \left(g(N_0) - l(N_0) \right) w_0 - \partial_t w_0 \right). \tag{41}$$

Plugging this term into equation (32) we obtain

$$\partial_t m_0 + \mathbf{v} \cdot \nabla m_1 = \mathcal{L}[\lambda_0] m_2 + \mathcal{L}[\lambda_1] m_2^z - \alpha m_2 + \frac{\alpha q}{\omega} M_2 + \frac{q}{\omega} \left(g(N_0) - l(N_0) \right) \frac{\alpha}{\beta} M_0 - \frac{q}{\omega} \partial_t \left(\frac{\alpha}{\beta} M_0 \right) - l(N_0) m_0. \tag{42}$$

After integrating again with respect to $\mathbf{v}$ this yields

$$\partial_t M_0 + \int_V \mathbf{v} \cdot \nabla m_1 \; d\mathbf{v} = \left(g(N_0) - l(N_0) \right) \frac{\alpha}{\beta} M_0 - \frac{\alpha}{\beta} \partial_t M_0 - l(N_0) M_0. \tag{43}$$

Rearranging gives

$$\partial_t \left(1 + \frac{\alpha}{\beta} \right) M_0 + \nabla \cdot \int_V \mathbf{v} m_1 \; d\mathbf{v} = \frac{\alpha}{\beta} g(N_0) M_0 - \left(1 + \frac{\alpha}{\beta} \right) M_0 l(N_0). \tag{44}$$

With the defined macroscopic quantity

$$N_0 = \left(1 + \frac{\alpha}{\beta} \right) M_0 \tag{45}$$

we obtain

$$\partial_t N_0 + \nabla \cdot \int_V \mathbf{v} m_1 \; d\mathbf{v} = \frac{\alpha}{\alpha + \beta} g(N_0) N_0 - N_0 l(N_0). \tag{46}$$

Now evaluate $\int_V \mathbf{v} m_1 d\mathbf{v}$. Recall

$$m_1 = -\frac{1}{\lambda_0+\alpha}\left(\mathbf{v}\cdot\nabla\left(\frac{q}{\omega}M_0\right)+\lambda_1 m_1^z\right). \tag{47}$$

Writing $g(\mathbf{x}) = \frac{1}{k^+A+k^-+\lambda_0+\alpha}$ and hence $m_1^z = g(\mathbf{x})f'(A)\mathbf{v}\cdot\nabla A\ m_0$ we have

$$m_1 = -\frac{1}{\lambda_0+\alpha}\left(\mathbf{v}\cdot\nabla\left(\frac{q}{\omega}M_0\right)+\lambda_1 g(\mathbf{x})f'(A)\mathbf{v}\cdot\nabla A\frac{q}{\omega}M_0\right). \tag{48}$$

It follows

$$\nabla\cdot\int_V \mathbf{v}m_1\ d\mathbf{v} = \nabla\cdot\left(-\frac{1}{\lambda_0+\alpha}\int_V \mathbf{v}\mathbf{v}^t\nabla\left(\frac{q}{\omega}M_0\right)d\mathbf{v}\right)+\nabla\cdot\left(\frac{\lambda_1}{\lambda_0+\alpha}\int_V \mathbf{v}\mathbf{v}^t\frac{q}{\omega}\ d\mathbf{v}g(\mathbf{x})f'(A)\nabla A M_0\right) \tag{49}$$

$$= \nabla\cdot\left(-\frac{1}{\lambda_0+\alpha}\nabla\cdot\left(\frac{1}{\omega}\int_V \mathbf{v}\mathbf{v}^t q\ d\mathbf{v}\ M_0\right)\right)+\nabla\cdot\left(\frac{\lambda_1}{\lambda_0+\alpha}g(\mathbf{x})f'(A)\frac{1}{\omega}\int_V \mathbf{v}\mathbf{v}^t q\ d\mathbf{v}\ \nabla A M_0\right). \tag{50}$$

Finally, we obtain with $M_0 = \frac{\beta}{\alpha+\beta}N_0$ and

$$\mathbb{D}_T(\mathbf{x}) = \frac{1}{\omega}\int_V \mathbf{v}\mathbf{v}^t q\ d\mathbf{v}. \tag{51}$$

the evolution equation

$$\partial_t N_0 - \nabla\cdot\left(\frac{1}{\lambda_0+\alpha}\nabla\cdot\left(\frac{\beta}{\alpha+\beta}\mathbb{D}_T(\mathbf{x})N_0\right)\right)+\nabla\cdot\left(\frac{\lambda_1}{\lambda_0+\alpha}g(\mathbf{x})f'(A)\frac{\beta}{\alpha+\beta}\mathbb{D}_T(\mathbf{x})\cdot\nabla A\ N_0\right)$$
$$= \frac{\alpha}{\alpha+\beta}g(N_0)N_0 - N_0 l(N_0). \tag{52}$$

Notice that we still have to determine the form of q in order to obtain explicit expressions for the tumor diffusion tensor $\mathbb{D}_T(\mathbf{x})$.

2.4 Determination of the coefficients

Now we are interested in the form of the diffusion tensor $\mathbb{D}_T(\mathbf{x})$ in equation (52). To determine its specific form we have to choose a concrete form for the fibre distribution q. As shown in [12], a possible choice can be

$$q(\mathbf{x},\boldsymbol{\theta}) = \frac{n}{|\mathbb{S}^{n-1}|\operatorname{tr}\mathbb{D}_W(\mathbf{x})}\boldsymbol{\theta}^t\mathbb{D}_W(\mathbf{x})\boldsymbol{\theta}. \tag{53}$$

The tensor $\mathbb{D}_W(\mathbf{x})$ is the *water diffusion tensor* and can be obtained for each voxel $\mathbf{x}$ by DTI measurements. This formula allows for computing the fibre distribution function for each voxel. In [12] it has been shown that for the choice (53) for the distribution q the tensor (51) has the form

$$\mathbb{D}_T(\mathbf{x}) = \frac{s^2}{\lambda_0(n+2)}\left(\mathbb{I}_n + 2\frac{\mathbb{D}_W(\mathbf{x})}{\operatorname{tr}\mathbb{D}_W(\mathbf{x})}\right). \tag{54}$$

The rates α and β are assumed not to vary drastically within the brain, and are hence constant in space.

2.5 The full macroscopic model

For the sake of clarity we collect the results of our calculations and formulate the whole macroscopic model again. We obtained from our scaling an approximating partial differential equation of advection-diffusion-reaction type for the macroscopic cell density N_0. We assume that the rates α and β do not vary in space and furthermore assume that the proliferation behaves logistic. Specifying g and l to be of the form

$$g(N_0) = c_g, \quad l(N_0) = c_l N_0,$$

with appropriate positive constants $c_g, c_l \in \mathbb{R}$, we obtain the equation

$$\partial_t N_0 - c_D\nabla\nabla\left(\mathbb{D}_T(\mathbf{x})N_0\right) - \lambda_1 c_D\nabla\left(\mathbf{u}(\mathbf{x})N_0\right) = \frac{\alpha}{\alpha+\beta}c_g N_0 - c_l N_0^2, \tag{55}$$

with $c_D = \frac{\beta}{(\lambda_0+\alpha)(\alpha+\beta)}$ and $\mathbf{u}(\mathbf{x}) = g(\mathbf{x})f'(A(\mathbf{x}))\mathbb{D}_T(\mathbf{x})\nabla A N_0$.

3 Numerical simulations

We present 2D simulations of the resulting macroscopic advection-diffusion-reaction equation (55). The tumor diffusion tensor, the tumor drift velocity and the local growth rates are precalculated using MATLAB[3]. The simulations of the macroscopic evolution equation are implemented using the DUNE framework [2].

The macroscopic quantities $\mathbb{D}_T(\mathbf{x})$ and $\mathbf{v}(\mathbf{x})$ are spatially dependent, and we expect regions in space where the system is diffusion dominated and regions where it is drift dominated. This can be expressed by the spatially dependent Péclet number $\mathrm{Pe} = \frac{\|\mathbf{v}(\mathbf{x})L\|}{\|\mathbb{D}_T(\mathbf{x})\|}$, where the norm in the numerator is the L^2 norm, while we take in the denominator the Frobenius norm of $\mathbb{D}_T$. L is a macroscopic characteristic length scale (i.e. a mesh width of 2 mm, in our present setting and simulations). For $\mathrm{Pe} \ll 1$ we have a diffusion dominated case, and classical methods for parabolic equations will apply, while for $\mathrm{Pe} \gg 1$ the equation is drift dominated, and hyperbolic numerical methods need to be used. Note that the equation is still parabolic, but the numerical method should be chosen based on its characteristics scales.

The numerical scheme needs to be able to handle non-linear degenerated anisotropic parabolic equations and full tensors. Furthermore it should be locally mass conservative. For these reasons we decided to employ a first order discontinuous Galerkin (dG) scheme in space and an implicit Euler scheme in time. The non-linearities are handled using an outer Newton scheme for each time step. This method is overall first order accurate.

3.1 Spatial Discretization

For the spatial discretization we use a structured mesh $\mathcal{M}(\Omega) = \{E_i\}$, which is a subset of the voxel mesh of the DTI data. Since our mesh is Cartesian with mesh-width h, the sets E_i are simply the grid cells that belong to the brain tissue. We define the skeleton of $\mathcal{M}$ as the boundary between those grid cells, $\Gamma = \{\gamma_{e,f} = \partial E_e \cap \partial E_f \mid E_e, E_f \in \mathcal{M},\ E_e \neq E_f,\ \text{and } |\gamma_{e,f}| > 0\}$.

We use a symmetric interior penalty discontinuous Galerkin method (SIPG) [36] as implemented in DUNE [2]. We denote with V_h the dG trial- and test space, which is in our case the space of piecewise bilinear polynomials

$$V_h = \left\{ \nu_h \in L^2(\Omega) \,:\, \nu_h|_E \in Q_1(E), E \in \mathcal{M}(\Omega) \right\},$$

where $Q_1(E)$ denotes the set of bilinear functions on E.

We test the above equation (55) with these ansatz functions, use a weak formulation, and express coupling conditions along the skeleton through jumps $[\![\, \cdot \,]\!]$ and averages $\{\, \cdot \,\}$ in a similar notation as in [1]. We use weighted averages, as proposed in [14]. Omitting the computational details, which can be found for example in [1], the resulting semi-discrete problem reads:

Find $N_{0h}(t) \in V_h$ such that

$$\partial_t N_{0h}(t) + a_h\big(N_{0h}(t), \nu_h\big) + J_h\big(N_{0h}(t), \nu_h\big) = R(N_{0h}) \qquad \forall \nu_h \in V_h, \tag{56}$$

with a nonlinear reaction term R, the bilinear form a_h, and a penalty term J_h given by

$$R(N_{0h}(t)) = \frac{\alpha}{\alpha+\beta} c_g N_{0h}(t) - c_l N_{0h}(t)^2, \tag{57}$$

$$\begin{aligned} a_h\big(N_{0h}(t), \nu_h\big) = &\int_\Omega \mathbb{D}_T \nabla N_{0h}(t) \cdot \nabla \nu_h \, dx - \int_\Gamma [\![\, N_{0h}(t) \,]\!] \cdot \{\, \mathbb{D}_T \nabla \nu_h \,\} \\ &+ [\![\, \nu_h \,]\!] \cdot \{\, \mathbb{D}_T \nabla N_{0h}(t) \,\} \, ds - \int_\Omega \mathbf{v}\, N_{0h}(t)\, \nabla \nu_h \, dx \\ &+ \int_\Gamma [\![\, \nu_h \,]\!] \cdot \mathbf{v}\, N_{0h}^{\uparrow}(t) ds, \end{aligned} \tag{58}$$

and

$$J_h\big(N_{0h}(t), \nu_h\big) = \eta h^{-1} \int_\Gamma [\![\, N_{0h} \,]\!] [\![\, \nu_h \,]\!] \, ds\,, \tag{59}$$

where $\eta > 0$ denotes the penalty factor. For a good choice of η we refer to [14].

[3] MATLAB Release 2012b, The MathWorks, Inc., Natick, Massachusetts, United States.

Note that we require the normal velocity to be continuous, i.e. $\mathbf{v}|_{\partial E_n}\mathbf{n}_n = -\mathbf{v}|_{\partial E_m}\mathbf{n}_m$, where $\mathbf{n}_n$ denotes the outer normal vector of grid cell E_n. To ensure this, we use a Raviart-Thomas RT0 approximation of the velocity field. On an internal edge with two adjacent cells E_n and E_m we define $[\![x]\!] = x|_{\partial E_n}\mathbf{n}_n + x|_{\partial E_m}\mathbf{n}_m$ and $\{ x \} = \omega_n x|_{\partial E_n} + \omega_m x|_{\partial E_m}$, with weights ω_n, ω_m and the unit outer normal vectors $\mathbf{n}_n, \mathbf{n}_m$. To be robust with respect to heterogeneous diffusion coefficients, we use the weights $\omega_n = \frac{\mathbf{n}_n^t \mathbb{D}_{Tn}\mathbf{n}_n}{\mathbf{n}_n^t(\mathbb{D}_{Tn}+\mathbb{D}_{Tm})\mathbf{n}_n}$ and $\omega_m = \frac{\mathbf{n}_m^t \mathbb{D}_{Tm}\mathbf{n}_m}{\mathbf{n}_m^t(\mathbb{D}_{Tn}+\mathbb{D}_{Tm})\mathbf{n}_m}$ respectively, where $\mathbb{D}_{Tn}$ denotes the tumor diffusion tensor computed in E_n. Note that due to $\mathbf{n}_n = -\mathbf{n}_m$ the relation $\omega_n + \omega_m = 1$ holds.
The advective term is stabilized using an upwind formulation, with the upwind reconstruction $N_{0h}^{\uparrow}$ of the cell density.

3.2 Temporal Discretization

For the time discretization of N_{0h} we use an implicit Euler scheme and choose the time step width τ such that the discrete CFL (Courant-Friedrichs-Lewy) condition of 1 is satisfied.
For each time step we obtain a non-linear system, due to the growth term. The modeling of the growth term requires that the tumor cell density is positive. The employed dG scheme is not monotone, small undershoots are possible and will occur in practice. Therefore we cannot directly compute $R(N_0)$, but employ a clipping at zero. The non-differentiability of the clipped operator at zero leads to severe problems in the Newton method. Thus, we additionally regularize the clipping with a parameter ϵ, which yields the clipping operator

$$C_\epsilon(N_0) = \begin{cases} 0 & \text{if } N_0 < 0 \\ {N_0}^2/\epsilon & \text{if } N_0 < 0.5\epsilon \\ N_0 - 0.25\epsilon & \text{else}\,. \end{cases} \tag{60}$$

For a time step $k+1$, $k \in [1, N)$, and a discrete time step width of τ, the fully discrete problem now reads: Find $N_{0h}^{k+1} \in V_h$ such that

$$\frac{1}{\tau} M_h N_{0h}^{k+1} + a_h(N_{0h}^{k+1}, \nu_h) + J_h(N_{0h}^{k+1}, \nu_h) - R(C_\epsilon(N_{0h}^{k+1})) = \frac{1}{\tau} M_h N_{0h}^{k} \qquad \forall \nu_h \in V_h. \tag{61}$$

After linearization of R we can employ a standard Newton scheme. To solve the linearized system a conjugate gradient method with an ILU precoditioner with zero-fill-in is applied.
Table 1 shows the parameter values used in the simulations.

Parameter	Value	Source
R_0	10^5	[3]
s	$10^{-6}\frac{\mathrm{m}}{\mathrm{s}}$	[29]
λ_0	$0.1\frac{1}{\mathrm{s}}$	[29]
λ_1	$0.01\frac{1}{\mathrm{s}}$	estimated
k^+	$0.1\frac{1}{\mathrm{s}}$	estimated
k^-	$0.1\frac{1}{\mathrm{s}}$	[24]
α	$10^{-2}\frac{1}{\mathrm{s}}$	estimated
β	$10^{-2}\frac{1}{\mathrm{s}}$	estimated
r_g	$10^{-5}\frac{1}{\mathrm{s}}$	source
r_l	$10^{-7}\frac{1}{\mathrm{s}}$	source

Table 1: Choice of parameters used for simulations.

3.3 Simulation results

The choice of appropriate terms for the gain and loss functions g and l is still an issue. When assuming -as in the most existing works on the macroscale- that cellular proliferation can be described with a logistic growth, the choice to make is to let $g(N_0) = r$ be constant for the proliferation rate $r_g \in \mathbb{R}^+$ and $l(N_0) = r_l N_0$ for $r_l \in \mathbb{R}^+$. Altogether this leads to the reaction term

$$\frac{\alpha}{\alpha+\beta} r_g N_0 - r_l N_0^2 = \left(\frac{\alpha}{\alpha+\beta} r_g - r_l N_0 \right) N_0.$$

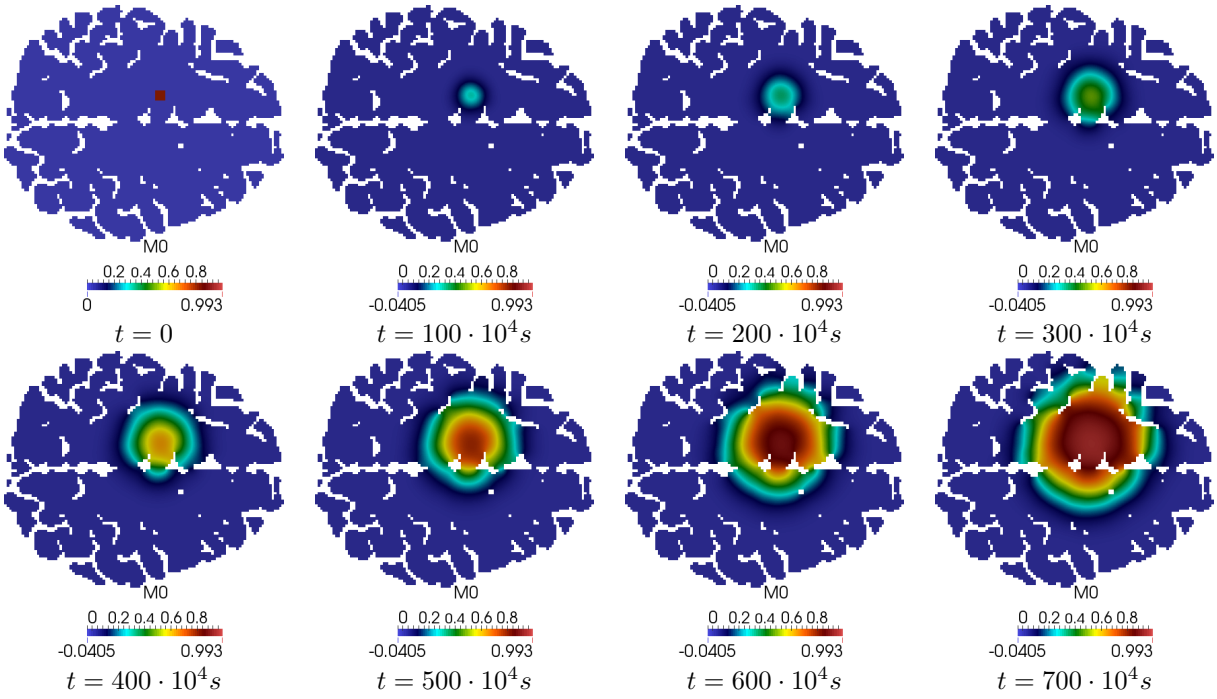

Figure 1: Simulation of the evolution equation: case involving subcellular dynamics with von Mises distribution with $\kappa = 20$.

Simulations of this model have been perfomed on a horizontal brain slice with a binary inital tumor placed in the left hemisphere. Figures 1 and 2 show simulations for the pure diffusion case and for the full system including haptotactic drift. As expected, proliferation causes sharper gradients compared to the advection-diffusion model without proliferative effects. The corresponding tumor growth patterns evolve faster than the patterns without proliferation. However, for the pure diffusion case the patterns do not differ significantly from the models without proliferation and, again, significant anisotropic behavior caused merely by diffusion cannot be observed.
Adding the haptotactic drift terms leads to branched structures, as Figure 2 shows. Obviously, the tumor spreads predominatly in brain white matter; from the clinical point of view these finger-like patterns are more realistic than an isotropic spread.

4 Discussion

The DTI-based multiscale model for glioma invasion proposed and analyzed in this work is an extension of the one introduced in [12]. The novelty is here that we account for proliferation of tumor cells. Thereby, we made use of the go and grow hypothesis and identified the resting cells with those proliferating. The choice of gain and loss functions $g(N)$ and $l(N)$ due to cell proliferation and death, as well as of the stopping (growth) rates can be done in a less restrictive way, leading -after the scaling- on the macroscale to rather general proliferation terms, of which the logistic growth (which is commonly chosen when writing some partial differential equations for tumor invasion directly on the population level) is merely a particular case.
The numerical simulations of the macroscopic equation show a highly anisotropic spread of the tumor cells, according to the underlying brain structure. As before in [12] this was achieved by the multiscality of our model (in particular the inclusion of subcellular receptor binding processes and their involvement in the cell turning rates), which led to the dominant haptotactic term in equation (55). When simulating only the pure diffusion model the corresponding invasive behavior is not as known from practice, where branched, fingering patterns like those in Figure 2 are observed. When compared with our previous multiscale model without proliferation in [12] the present setting predicts -as expected- a faster invasion, with larger cell clusters.
The nontrivial issue of modeling cell proliferation in a way which is less artificial than just choosing it to be a logistic growth on the macrolevel was handled here by accounting for the resting (and hence dividing) cells. This, however, does not seem to be the only way to characterize it. Bellomo et al. [4, 5, 6]

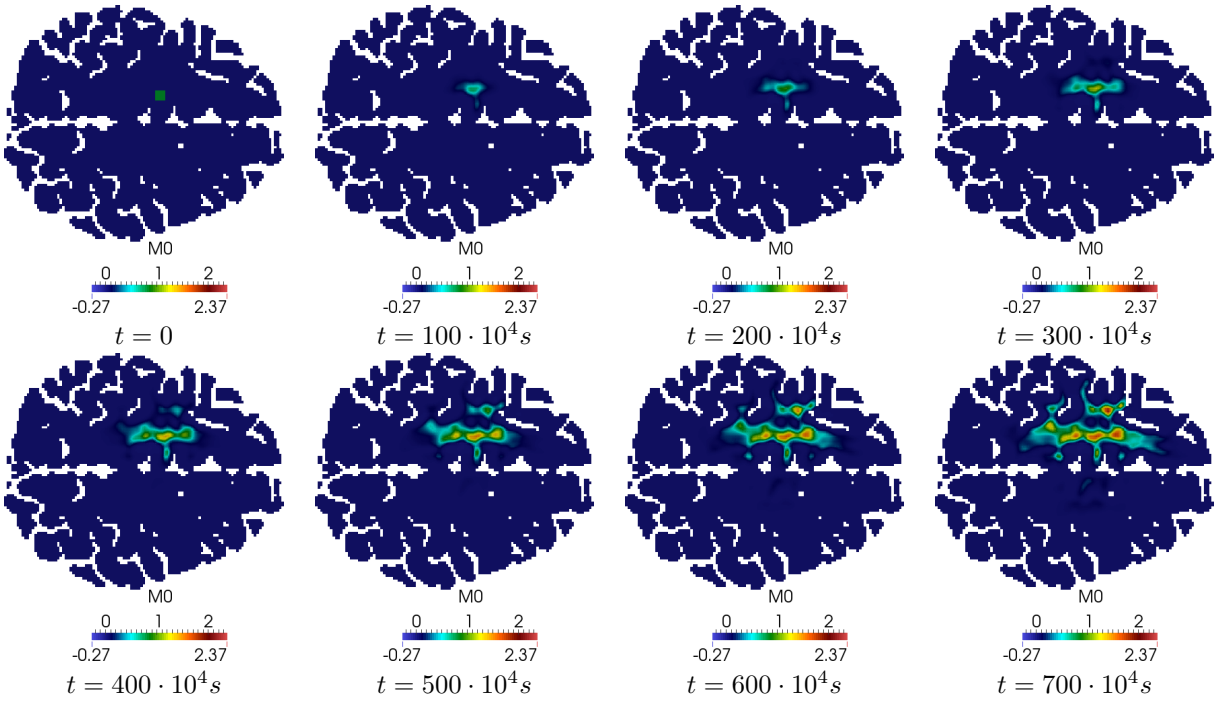

Figure 2: Simulation of the evolution equation: case involving subcellular dynamics with von Mises distribution with $\kappa = 20$.

proposed to model proliferation on the mesolevel by letting the cells with different internal states[4] interact with each other, which is arguable, as cancer cells can divide without needing to stay in touch with their neighbours. The modeling of cell proliferation on the mesolevel and the deduction of the appropriate mesoscopic equation are thus an aim to follow.

Acknowledgements

We thank Carsten Wolters and Felix Lucka (Institute of Biomagnetism and Biosignalanalysis, University of Münster) for the preprocessed DTI data and their advice with the visualization software SciRun.

References

[1] D. N. Arnold, F. Brezzi, B. Cockburn, and L. D. Marini. Unified Analysis of Discontinuous Galerkin Methods for Elliptic Problems. *SIAM Journal on Numerical Analysis*, 39(5):1749–1779, 2002.

[2] P. Bastian, M. Blatt, A. Dedner, C. Engwer, R. Klöfkorn, R. Kornhuber, M. Ohlberger, and O. Sander. A generic grid interface for parallel and adaptive scientific computing. Part II: Implementation and tests in DUNE. *Computing*, 82(2–3):121–138, 7 2008.

[3] A.M. Belkin, G. Tsurupa, E. Zemskov, Y. Veklich, J.W. Weisel, and L. Medved. Transglutaminase-mediated oligomerization of the fibrin(ogen) αC domains promotes integrin-dependent cell adhesion and signaling. *Blood*, 105(9):3561–3568, 2005.

[4] N. Bellomo, A. Bellouquid, J. Nieto, and J. Soler. Complexity and mathematical tools toward the modeling of multicellular growing systems. *Mathematical and Computer Modelling*, 51:441–451, 2010.

[5] N. Bellomo, A. Bellouquid, J. Nieto, and J. Soler. On the asymptotic theory from microscopic to macroscopic tissue models: an overview with perspectives. *Math. Models Methods Appl. Sci.*, 22:Paper No. 1130001, 37 pages, 2012.

[6] N. Bellomo, D. Knopoff, and J. Soler. On the difficult interplay between life, "complexity", and mathematical sciences. *Math. Models Methods Appl. Sci.*, 23(10):1861–1913, 2013.

[4] in those papers these are called *activity variables*

[7] T. Beppu, T. Inoue, Y. Shibata, A. Kurose, H. Arai, K. Ogasawara, A. Ogawa, S. Nakamura, and H. Kabasawa. Measurement of fractional anisotropy using diffuson tensor MRI in supratentorial astrocytic tumors. *Journal of Neuro-Oncology*, 63:109–116, 2003.

[8] K. Böttger, H. Hatzikirou, A. Chauviere, and A. Deutsch. Investigation of the migration/proliferation dichotomy and its impact on avascular glioma invasion. *Mathematical Modelling of Natural Phenomena*, 7:105–135, 2012.

[9] M. Descoteaux. *High Angular Resolution Diffusion MRI: from Local Estimation to Segmentation and Tractography.* Ph.D. thesis, Université Nice-Sophia Antipolis, 2008.

[10] M. Descoteaux, R. Deriche, T. Knische, and A. Anwander. Deterministic and probabilistic tractography based on complex fibre orientation distribution. *IEEE Transactions of Medical Imaging*, 28(2):269–286, 2009.

[11] M. Descoteaux, R. Deriche, T.R. Knische, and A. Anwander. Deterministic and probabilistic tractography based on complex fibre orientation distributions. *IEEE Transactions on Medical Imaging*, 28:269–286, 2009.

[12] C. Engwer, T. Hillen, Knappitsch M., and Surulescu C. Glioma follow white matter tracts; a multiscale DTI-based model. preprint, University of Münster, submitted, 2013.

[13] R. Erban and H. Othmer. From signal transduction to spatial pattern formation in *e. coli*: a paradigm for multiscale modeling in biology. *Multiscale Modeling and Simulation*, 3(2):362–394, 2005.

[14] A. Ern, A. F. Stephansen, and P. Zunino. A discontinuous Galerkin method with weighted averages for advection-diffusion equations with locally small and anisotropic diffusivity. *IMA Journal of Numerical Analysis*, 29(2):235–256, 2009.

[15] A. Giese, M.A. Loo, N. Tran, D. Haskett, S. Coons, and M. Berens. Dichotomy of astrocytoma migration and proliferation. *International Journal of Cancer*, 67:275–282, 1996.

[16] D. Grünbaum. Advection-diffusion equations for internal state-mediated random walks. *SIAM Journal for Applied Mathemtics.*, 61:43–73, 2000.

[17] D. Hanahan and R.A. Weinberg. Hallmarks of cancer: the next generation. *Cell*, 144(5):646–674, 2011.

[18] H. Hatzikirou, D. Basanta, M. Simon, K. Schaller, and A. Deutsch. 'go or grow': the key to the emergence of invasion in tumour progression? *Math Med Biol*, 29:49–65, 2012.

[19] T. Hillen. Transport equations with restin phases. *European Journal of Applied Mathematics*, 14:613–636, 2003.

[20] T. Hillen and H. Othmer. The diffusion limit of transport equations derived from velocity jump processes. *SIAM Journal on Applied Mathematics*, 61(3), 2000.

[21] K.S. Hoek, O.M. Eichhoff, N.C. Schlegel, U. Döbbeling, S. Hemmi, and R. Dummer. In vivo switching of human melanoma cells between proliferative and invasive states. *Cancer Res.*, 68:650–656, 2008.

[22] J. Kelkel and C. Surulescu. On some models for cancer cell migration through tissue networks. *Mathematical Biosciences and Engineering*, 8(2):575–589, 2011.

[23] J. Kelkel and C. Surulescu. A multiscale approach to cell migration in tissue networks. *Mathematical Models and Methods in Applied Sciences*, 23(3), 2012.

[24] D.A. Lauffenburger and J.L. Lindermann. *Receptors. Models for binding, trafficking and signaling.* Oxford University Press, 1993.

[25] K.R. Legate, S.A. Wickström, and R. Fässler. Genetic and cell biological analysis of integrin outside-in signaling. *Genes Dev.*, 23:397–418, 2009.

[26] T. Lorenz and C. Surulescu. On a class of multiscale cancer cell migration models: Well-posedness in less regular function spaces. *Mathematical Models and Methods in Applied Sciences*, 24, 2014.

[27] G. Meral, C. Stinner, and C. Surulescu. On a multiscale model involving cell contractivity and its effects on tumor invasion. *preprint TU Kaiserslautern, submitted.*, 2013.

[28] G. Meral and C. Surulescu. Mathematical modelling, analysis and numerical simulations for the influence of the heat shock proteins on tumour invasion. *Journal of Math. Anal. Appl.*, 408:597–614, 2013.

[29] M. Sidani, D. Wessels, G. Mouneimne, M. Ghosh, S. Goswami, C. Sarmiento, W. Wang, S. Kuhl, M. El-Sibai, J.M. Backer, R. Eddy, D. Soll, and J. Condeelis. Cofilin determines the migration behavior and turning frequency of metastatic cancer cells. *The Journal of Cell Biology*, 179(4):777–791, 2007.

[30] C. Stinner, C. Surulescu, and G. Meral. A multiscale model for ph-tactic tumor invasion with time-varying carrying capacities. *preprint TU Kaiserslautern*, 2014.

[31] C. Stinner, C. Surulescu, and M. Winkler. Global weak solutions in a pde-ode system modeling multiscale cancer cell invasion. *preprint TU Kaiserslautern, submitted.*, 2013.

[32] P.C. Sundgren, Q. Dong, D. Gomez-Hassan, S.K. Mukherji, P. Maly, and R. Welsh. Diffusion tensor imaging of the brain: review of clinical applications. *Neurocarciology*, 46:339–350, 2004.

[33] Z. Szymanska, J. Urbanski, and A. Marciniak-Czochra. Mathematical modelling of the influence of heat shock proteins on cancer invasion of tissue. *Journal of Mathematical Biology*, 58:819–844, 2009.

[34] D.S. Tuch. Q-ball imaging. *Magnetic resonance in Medicine*, 52(6):1358–1372, 2004.

[35] D.S. Tuch, T.G. Reese, M.R: Wiegell, and V.J. Wedeen. Diffusion mri of compelx neural architecture. *Neuron*, 40:885–895, 2003.

[36] M. F. Wheeler. An Elliptic Collocation-Finite Element Method with Interior Penalties. *SIAM Journal on Numerical Analysis*, 15(1):152–161, 1978.

[37] M. Wrensch, Y. Minn, T. Chew, M. Bondy, and M.S. Berger. Epidemiology of primary brain tumors: Current concepts and review of the literature. *Neuro-Oncology*, 4(4):278–299, 2002.